



Cooperative action of separate interaction domains promotes high-affinity DNA binding of *Arabidopsis thaliana* ARF transcription factors

Mattia Fontana^{ab} , Mark Roosjen^b, Isidro Crespo García^c , Willy van den Berg^b , Marc Malfois^c , Roeland Boer^c , Dolf Weijers^{b,1} , and Johannes Hohlbein^{a,d,1}

Edited by Mark Estelle, University of California at San Diego, La Jolla, CA; received November 22, 2022; accepted February 6, 2023

The signaling molecule auxin coordinates many growth and development processes in plants, mainly through modulating gene expression. Transcriptional response is mediated by the family of auxin response factors (ARF). Monomers of this family recognize a DNA motif and can homodimerize through their DNA-binding domain (DBD), enabling cooperative binding to an inverted binding site. Most ARFs further contain a C-terminal PB1 domain that is capable of homotypic interactions and mediating interactions with Aux/IAA repressors. Given the dual role of the PB1 domain, and the ability of both DBD and PB1 domain to mediate dimerization, a key question is how these domains contribute to DNA-binding specificity and affinity. So far, ARF-ARF and ARF-DNA interactions have mostly been approached using qualitative methods that do not provide a quantitative and dynamic view on the binding equilibria. Here, we utilize a DNA binding assay based on single-molecule Förster resonance energy transfer (smFRET) to study the affinity and kinetics of the interaction of several *Arabidopsis thaliana* ARFs with an IR7 auxin-responsive element (AuxRE). We show that both DBD and PB1 domains of AtARF2 contribute toward DNA binding, and we identify ARF dimer stability as a key parameter in defining binding affinity and kinetics across AtARFs. Lastly, we derived an analytical solution for a four-state cyclic model that explains both the kinetics and the affinity of the interaction between AtARF2 and IR7. Our work demonstrates that the affinity of ARFs toward composite DNA response elements is defined by dimerization equilibrium, identifying this as a key element in ARF-mediated transcriptional activity.

protein-DNA interaction | transcription factor | smFRET | auxin response factor | four-state cyclic model

The plant signaling molecule auxin plays a major role in many cellular and developmental processes. Auxin triggers both non-transcriptional and transcriptional responses with the latter being controlled by the nuclear auxin pathway (1–5). This pathway involves three main players: the transcription factor auxin response factor (ARF), its repressor auxin/indole-3-acetic acid (Aux/IAA), and the ubiquitin ligase complex SCF^{TIR1/AFB}. Binding of auxin to TIR1/AFB enables the recognition and ubiquitination of Aux/IAA. Upon degradation of Aux/IAA, ARF is able to modulate the expression of its downstream target genes.

The interaction between ARFs and Aux/IAAs is mediated by the C-terminal Phox and Bem1p (PB1) domain present in both proteins. The PB1 domain features two oppositely charged surfaces (type I/II or AB [acid basic] PB1 domain) that can undergo head-to-tail oligomerization (6–9). Remarkably, this structural characteristic enables scenarios of homo- and hetero-oligomerization among and between Aux/IAAs and ARFs. In addition to the PB1 domain, ARFs consist of two other domains, the Middle Region (MR) and the N-terminal DNA Binding Domain (DBD). The MR domain is predicted to be intrinsically disordered (5) and its amino acid sequence differs between the three phylogenetically separated ARF clades (A, B, and C) (10, 11). When tested for their effect on gene expression, some ARFs activate auxin-responsive genes while other repress them. In general, class A ARFs (e.g., *Arabidopsis thaliana* ARF5) act as activators while class B (e.g., *A. thaliana* ARF1 and 2) and C ARFs act as repressors (10). The DBD domain physically interacts with its DNA response element (RE) called AuxRE (auxin-responsive element) (12). This cis-regulatory element was first identified in promoters of auxin-responsive genes in pea (13) and soybean (14, 15) and was found to be essential for their auxin-inducibility. The canonical TGTCTC recognition sequence was later shown to be bound by different members of the ARF family (12, 16). More recently, the TGTCCG recognition sequence was found to have an even higher affinity for ARFs in vitro (17–19) and was used to create an enhanced artificial auxin response reporter (20). Single AuxREs are bound by single ARF

Significance

The signaling molecule auxin controls many aspects of plant development and growth. At the center of its signaling pathway lies the family of transcription factors called auxin response factors (ARF). These proteins recognize specific DNA elements in plant genes and modulate their expression. Most members of the ARF family contain two domains capable of homodimerization, the DNA binding domain (DBD) and the PB1 domain. An open question is how these different interactions contribute to conferring DNA-binding specificity and affinity. Here, the authors employ a single-molecule DNA-binding assay to study the affinity and kinetics of the interaction between several ARFs and a DNA element. This work shows that this interaction can be tuned by small changes of ARFs dimerization equilibrium.

Author contributions: M.F., R.B., D.W., and J.H. designed research; M.F. and I.C.G. performed research; M.R., I.C.G., and W.v.d.B. contributed new reagents/analytical tools; M.F., I.C.G., M.M., R.B., D.W., and J.H. analyzed data; and M.F., D.W., and J.H. wrote the paper.

The authors declare no competing interest.

This article is a PNAS Direct Submission.

Copyright © 2023 the Author(s). Published by PNAS. This open access article is distributed under Creative Commons Attribution-NonCommercial-NoDerivatives License 4.0 (CC BY-NC-ND).

¹To whom correspondence should be addressed. Email: dolf.weijers@wur.nl or johannes.hohlbein@wur.nl.

This article contains supporting information online at <https://www.pnas.org/lookup/suppl/doi:10.1073/pnas.2219916120/-/DCSupplemental>.

Published March 7, 2023.

monomers but ARF DBDs can dimerize in solution and bind cooperatively to composite response elements bearing two AuxRE's in an inverted configuration (inverted repeat, IR) (19, 21); moreover, ARF dimerization through its DBD is necessary for ARF function in vivo (19, 21). It was proposed that ARFs may differ in their preference for the space tolerated between inverted AuxRE sites (19) but analysis in a yeast model suggests that additional factors may influence ARF–DNA binding specificity (22), and genome-wide in vitro binding assays in maize also suggest extensive similarities in binding among ARFs (23). Interestingly, the PB1 domain seems to have diverse effects on different class A ARFs as its deletion in *Marchantia polymorpha* ARF1 generates a loss-of-function mutant (24), whereas in *A. thaliana* ARF5, the mutant maintains its function and is hyperactive (25). The effect of the homotypic interaction of ARF PB1 domains of another class A ARF, AtARF19, has been studied using synthetic auxin response circuits in yeast, showing that mutating either the positive or the negative side of the PB1 domain reduces its ability to promote transcription (26).

Although many structures and relevant interactions among the various components of the auxin nuclear pathway have been identified, quantitative data on the affinity and kinetics of these interactions have remained scarce. In particular, the effects of the dimer/monomer equilibrium on the interaction between ARFs and between ARFs and AuxREs, or the effect of mutations on the DBD and PB1 domains on ARF dimerization have not yet been systematically studied. Particularly, it is unclear whether and how both interaction domains (DBD and PB1) contribute to DNA binding, and what their relative contributions are. Furthermore, it is unclear whether oligomerization of ARF PB1 domains contributes to DNA binding.

Here, we employed a DNA-binding assay based on single-molecule Förster resonance energy transfer (smFRET) to quantitatively assess the binding affinities between different *A. thaliana* ARFs and a response element composed of two AuxREs in an inverted repeat configuration with a spacing of seven base pairs (IR7). We found that while the DNA-binding domain alone can bind DNA, the presence of the PB1 domain increases the affinity of AtARF2 toward the tested composite response element. In fact, this effect can be ascribed to increased stability of the dimer, whereas AtARF2 oligomerization has no sizable effect. We introduce a general four-state cyclic model to quantify the mechanisms of ARF interaction with the bipartite DNA response element; the simultaneous analysis of the affinity and kinetics data using this model revealed that the increase in affinity can be completely pinned to the shift in the dimer–monomer equilibrium. Further analysis of variants of AtARF5-DBD and other AtARF-DBDs showed that changes in dimer stability generated by changes in the DBD domain display the same pattern on the kinetics as the ones generated by changes in the PB1 domain, highlighting that stable protein dimers ensure high-affinity DNA binding, no matter the source of their stability.

Results

The AtARF2 PB1 Domain Promotes DNA Binding through Stabilization of the AtARF2 Dimer. A ChIP experiment on *A. thaliana* ARF19 expressed in yeast (26) suggested that PB1 mutations affect DNA-binding affinity. To test whether a similar dependency for DNA binding on the distal PB1 domain exists in the isolated protein, we purified the Arabidopsis ARF2 protein (B-class) and asked whether the interactions between the PB1 domains modulate affinity of ARFs toward a composite AuxRE in vitro. We designed smFRET experiments in which the binding of ARFs to a small doubly labeled double-stranded DNA (dsDNA) oligo containing two AuxREs in

an inverted configuration spaced by seven base pairs (IR7) leads to a decrease of FRET efficiency (Fig. 1A and *SI Appendix*, Fig. S1). We then performed titrations with increasing concentrations of different AtARF2 variants (Fig. 1B). The ARF DBD alone is sufficient for cooperative DNA binding to the IR7 element (19); to explore the influence of regions outside the DBD, we first compared binding of AtARF2-DBD and full-length AtARF2 (FL; DBD-MR-PB1). The FRET efficiency distributions of the DNA sensor show the free DNA population (93% occupancy) centered at $E^* = 0.59$ in the absence of ARF proteins. With increasing concentration of AtARF2-DBD or AtARF2-FL, the low FRET population representing the ARF-bound DNA fraction (centered at $E^* = 0.42$) becomes progressively more populated. To demonstrate that the shift seen during the titration is generated by specific binding of ARF to the DNA and that the binding is reversible, we performed a washing step at the end of each titration that reverted the FRET efficiency distributions to the ones seen in the absence of ARF. When comparing AtARF2-DBD and AtARF2-FL, the FRET efficiency distributions clearly show the effect of the PB1 domain on the interaction between ARF2 and the IR7 response element; the shift between the response element being mostly free to mostly bound occurs at a protein concentration almost one order of magnitude lower with the full-length protein (256 to 512 nM AtARF2-DBD vs. 32 to 64 nM AtARF2-FL). This finding is consistent with the PB1 domain promoting DNA binding. However, the full-length ARF protein also contains an extended MR region. To address the role of the PB1 domain specifically, we engineered mutations in the PB1 domain that prevent head-to-tail interaction: AtARF2-FL K2S (K737S) and AtARF2-FL OPCA (D797-8S) carry mutations of amino acids on the positive (K2S) and negative (OPCA motif) sides of the PB1 domain, respectively, both of which were shown to impair the interaction between PB1 domains (6). In both mutant ARF2 versions, we see equal percentages of DNA bound and free at concentrations close to the ones of AtARF2-DBD (64 to 128 nM K2S and 128 to 256 nM OPCA). Thus, PB1 domain interactions contribute to efficient DNA binding of isolated AtARF2 protein.

PB1 domains could potentially oligomerize through head-to-tail interactions. To address if oligomerization stabilizes DNA binding, we compared a mixture of AtARF2-FL K2S and AtARF2-FL-OPCA in a 1:1 ratio (henceforth AtARF2 FL KpO) with the wild-type version (ARF2-FL). While the latter allows for oligomerization, the former should only be able to dimerize. Both AtARF2-FL KpO and AtARF2-FL show high affinity toward the IR7 (32 to 64 nM). Taken together, these observations indicate that the PB1 domain stabilizes the binding of ARF2 toward an IR7 response element through stabilization of the protein dimer.

Modeling ARF–DNA Interactions. One way of quantifying the effect of the PB1 domain on the affinity between ARF and its RE is to fit the increase of the fraction of DNA-bound to ARF as the concentration of protein increases, with a single apparent K_d^* . This approach can reliably summarize the strength of the interaction providing a single numerical value that exemplifies at which endogenous protein concentration the interaction becomes relevant (24, 27), but fails to properly describe the underlying system, which results in a lack of predictive power.

The interaction between a protein that can dimerize and a bipartite response element on the DNA can be described using a four-state cyclic model. This model allows for monomers or dimers to bind the DNA, for monomers and dimers to exist in solution, and for dimers to form or dissociate both in solution or on the DNA. Fig. 1C depicts the model for AtARF2-FL KpO; the two AtARF2-FL variants are characterized by the same DBD (red) and MR (black) but are mutated on the two opposite surfaces of the PB1 domain (K2S and OPCA

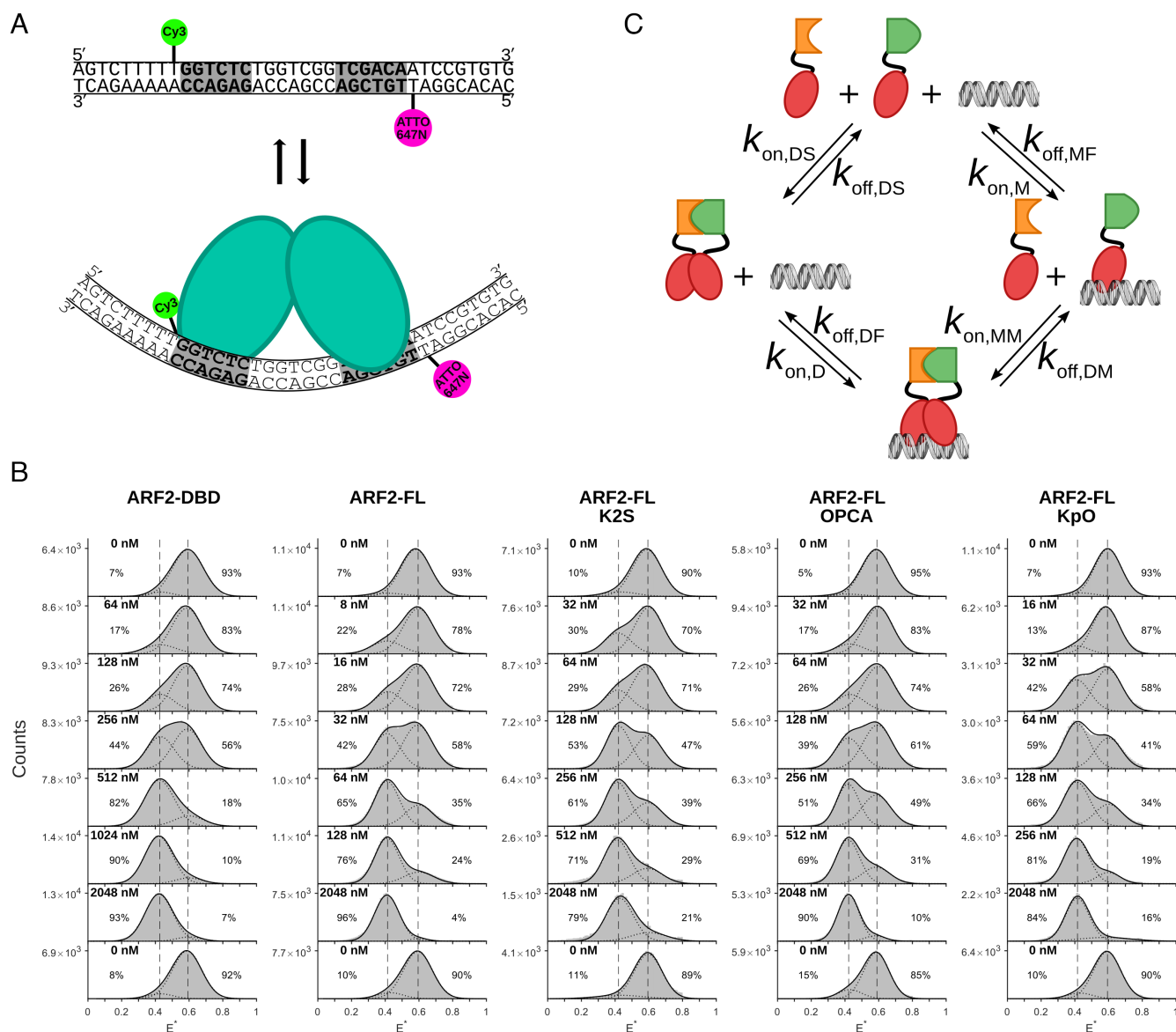


Fig. 1. SmFRET binding assay and four-state cyclic model. (A) Schematic representation of the DNA-binding assay used to evaluate ARF binding; the dsDNA is labeled with Cy3 and Atto647N on the opposite sides of the response element (RE). Upon protein binding, the increased distance between the dyes leads to a decrease in FRET efficiency. (B) Titrations of the dsDNA with several ARF variants. The dsDNA alone has a FRET efficiency $E^* = 0.59$; as the protein concentration increases the population of bound DNA (centered at $E^* = 0.42$) increases until all the DNA is bound (saturating condition). A washing step suffices to reset the system proving that the bound population is generated by specific and reversible binding of ARF. Vertical dashed lines are added for visual guidance. (C) Schematic representation of the four-state cyclic model for ARF2-FL KpO-IR7. Note that the dsDNA containing the DNA response element can be found in three states: free (F), bound to a monomer (M) and bound to a dimer (D). The two ARF2 full length variants (K2S and OPCA) have the same DBD domain (in red) and MR domain (in black) but their PB1 domain (in orange and green, respectively) carry a mutation on either one of the two different surfaces; this hinders oligomerization but allows dimerization. The binding of a dimer to a bipartite response element can occur either through two successive binding events of a monomer or through direct binding of a dimer formed in solution. The dissociation can occur either by the loss of a monomer followed by the dissociation of the second monomer from the DNA or by direct dissociation of a dimer from the DNA.

mutants in orange and green, respectively); this allows for the formation of PB1 domain dimers but hinders the formation of oligomers. The system is defined by four k_{on} s and four k_{off} s or, alternatively, by four equilibrium constants (K s). The presence of the PB1 domain should not change the contacting interface between the DBDs and the DNA; hence, the k_{off} of the dimer from the DNA ($k_{off,DF}$) should have the same value for all AtARF2-variants; the same holds for the k_{off} of the monomer from the DNA ($k_{off,MF}$). Moreover, the PB1 domain has limited influence on the k_{on} s of the system which stay diffusion limited. The only constants that are expected to be influenced by changes in the stability of the dimer induced by the PB1 domain are the ones associated with the separation of two monomers: the equilibrium dissociation constant of the dimer in solution

($K_1 = k_{off,DS} / k_{on,DS}$) and $k_{off,DM}$, which encompasses the stability of the dimer on the DNA. As the model is a closed cycle, microscopic reversibility (28) implies that only one of these two parameters is a free parameter; then, the different variants tested are characterized in this model by the single variant-specific parameter K_1 , which encompasses the stability of the ARF dimer. Fitting experimental results to determine K_1 and other relevant shared kinetic constants provides a deeper understanding of the system allowing to make prediction for other ARF-AuxRE interactions.

ARF-IR7 Interaction Follows a Four-State Cyclic Interaction Mechanism. To obtain the kinetics of AtARF2/IR7 interaction, we analyzed relevant data points of the titrations for the series of

variants using ebFRET (29), a MATLAB suite for empirical Bayes Hidden Markov Model (HMM) analysis of single-molecule time traces (*Materials and Methods*). As the DNA oligonucleotides are immobilized, their interaction with the proteins in solution can be monitored for several minutes (250 s in our experiments). The analyzed FRET traces returned the most probable hidden state sequence for each trace (Fig. 2A) according to the set of kinetic parameters that best explain the transitions and states seen in the entire dataset.

To facilitate the identification of transitions by ebFRET, we selected three concentrations of ARF ($[ARF]_T$) that returned close-to-equal populations of ARF-bound and free DNA for each AtARF2 variant. Each AtARF2 variant was tested in at least three independent titrations; each data point of each titration was analyzed independently using ebFRET and returned a value for k_{on} , a value for k_{off} and, from their ratio, a value for K_d (Fig. 2B, colored markers). The observed k_{on} shows a trend

in which ARF variants with higher affinity show faster association. On the other hand, the k_{off} shows similar values for all the FL variants whilst AtARF2-DBD has a faster k_{off} . The resulting K_d s show the expected trend, with AtARF2-DBD having the lowest affinity, AtARF2-FL KpO and wt showing the tightest binding, and AtARF2-FL K2S and OPCA having an affinity in between these. The trends seen in k_{on} and k_{off} suggest that the analysis of the kinetics using HMM is capturing the interaction between the ARF dimer and the DNA and that the interaction between an ARF monomer and the DNA occurs on a timescale shorter than the 500 ms acquisition time used in our experiments.

For a four-state cyclic model, the binding isotherm (Fig. 2C, colored markers) and observed kinetic constants (Fig. 2B, colored markers) can be fitted with a system of equations containing a set of three parameters shared across all AtARF2 variants ($k_{on,mic}$, $k_{off,DF}$, and $k_{off,MF}$) and the variant-specific parameter K_I

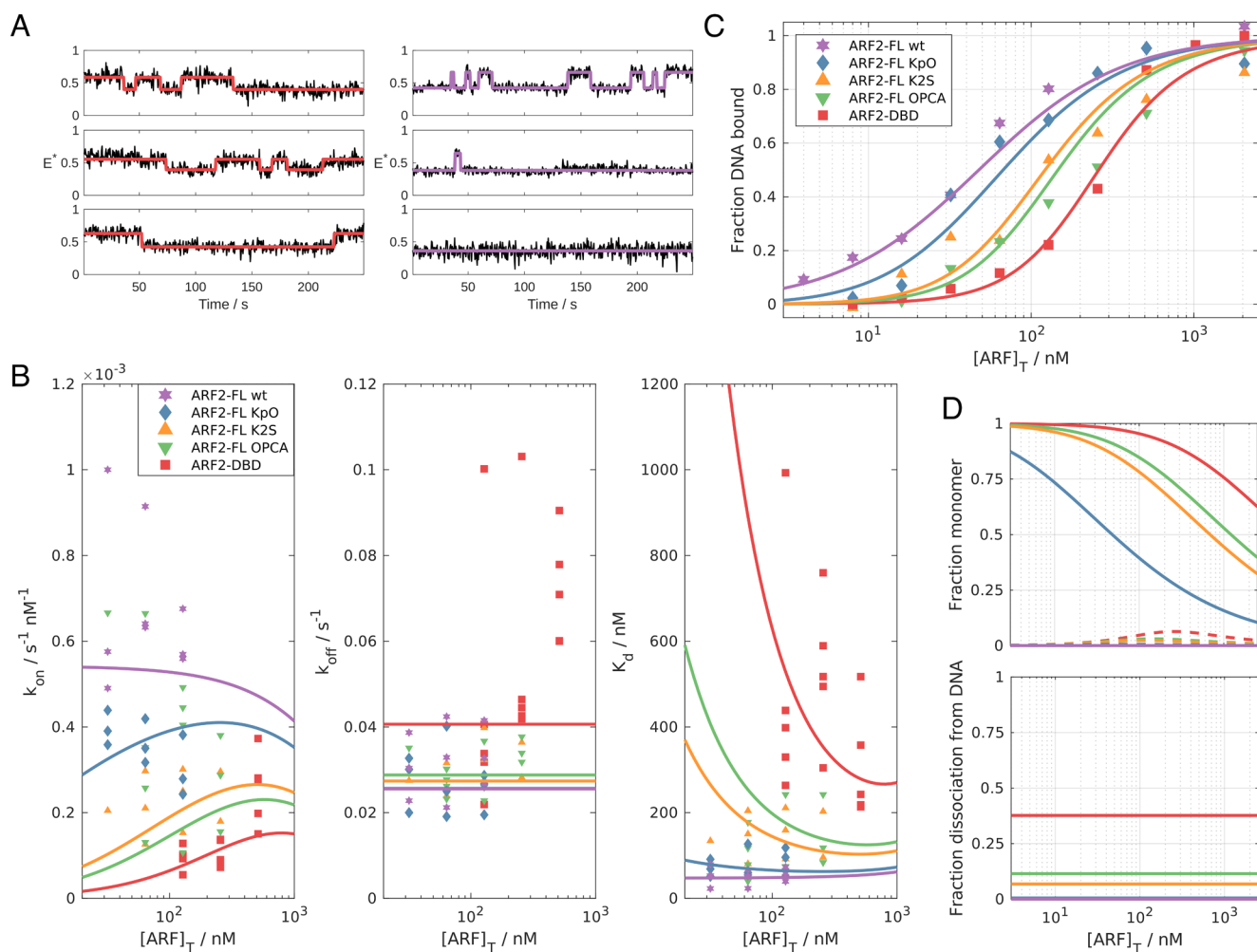


Fig. 2. AtARF2-IR7 interaction follows a four-state cyclic interaction mechanism. (A) Example of FRET efficiency time traces of individual doubly labeled dsDNA's in presence of 128 nM of either AtARF2-DBD (Left) or AtARF2-FL wt (Right). The FRET efficiency is reported in black and the most probable sequence of hidden states returned by ebFRET is represented in red (AtARF2-DBD) and purple (AtARF2-FL wt). (B) Kinetics parameters obtained from ebFRET. For each ARF variant three concentrations closest to having half of the DNA bound to ARF were measured in at least three independent titrations. Each repeat of each concentration is analyzed independently using ebFRET obtaining a value of observed k_{on} and k_{off} (and, from their ratio the K_d) and plotted using colored markers. (C) Fraction of DNA bound by ARF as function of ARF concentration (binding isotherm). The fractions bound were obtained from the histograms and plotted using colored markers (Fig. 1B and *Materials and Methods*). (B and C) The result of the global fit of the kinetics of binding and the fraction of DNA bound is reported as colored lines. (D) Features of the four states system as solved by the global fit. *Top:* In solution, the monomer is the most abundant species (solid lines). On the DNA, the monomer accounts for less than 10% of the bound DNA (dashed lines). *Bottom:* Fraction dissociation of the AtARF2 dimer from the DNA via loss of an AtARF2 monomer. The dissociation of the AtARF2 dimer from the DNA can occur either via its direct unbinding from the DNA or by initial loss of an AtARF2 monomer. Direct unbinding of the dimer is the predominant route for all AtARF2 variants but the fraction of dissociations happening via an initial loss of a monomer accounts for almost 40% of the events in case of AtARF2-DBD.

Table 1. Global fit: Values and uncertainty of the fitting parameters reported as mean (95% CI)

Protein	$k_{\text{on,mic}}$ [nM ⁻¹ s ⁻¹]	$k_{\text{off,MF}}$ [s ⁻¹]	$k_{\text{off,DF}}$ [s ⁻¹]	K_{I} [μM]
AtARF2-DBD	5.4 [3.6:7.3] × 10 ⁻⁴	1.7 [0.6:2.8]	2.6 [2.2:2.9] × 10 ⁻²	1.9 [0.9:2.9] × 10 ⁰
AtARF2-FL OPCA				4.1 [1.0:7.1] × 10 ⁻¹
AtARF2-FL K2S				2.3 [0.4:4.2] × 10 ⁻¹
AtARF2-FL KpO				1.6 [-1.5:4.7] × 10 ⁻²
AtARF2-FL wt				0.0 [-0.4:0.4] × 10 ⁻⁶

(SI Appendix, Note 1 and 2). Here, $k_{\text{on,mic}}$ is the microscopic k_{on} that a monomer displays when binding a single AuxRE and hence it is equal to $k_{\text{on,MM}}$ but it is half the value of $k_{\text{on,M}}$ and $k_{\text{on,D}}$.

The global fit (Fig. 2 B and C, colored lines) returned the values for $k_{\text{on,mic}}$, $k_{\text{off,DF}}$, $k_{\text{off,MF}}$, and K_{I} s that best explain the experimental data (Table 1). The global fit converged to a K_{I} of 0 nM for AtARF2-FL wt; in this situation, the equation of the fraction bound for the four-state system simplifies to a simple binding isotherm for the dimer (SI Appendix, Note 1). On the other binding isotherms, the fit captured the shift of the binding to higher $[\text{ARF}]_{\text{T}}$ thanks to increasing values of K_{I} , which corresponds to a decrease in dimer stability (Fig. 2C). The fit of the binding isotherm of AtARF2FL KpO is still very close to the one of AtARF2-FL wt but because of the decrease in dimer stability ($K_{\text{I}} = 0.016 \mu\text{M}$) its steepness is increased. The two AtARF2-FL mutants, K2S and OPCA, show similar values of K_{I} (0.23 μM and 0.41 μM respectively). Lastly, the fit returned a value of K_{I} of 1.9 μM for AtARF2-DBD.

Looking at the observed binding kinetics, the global fit captures the trends of the observed k_{on} and k_{off} (Fig. 2B). Here, AtARF2 variants with higher dimer stability display higher values of observed k_{on} as their lower K_{I} increases the effective concentration of ARF dimer in solution. The fits for the observed k_{off} of AtARF2-FL wt and KpO converge to the value of the dissociation kinetic of the dimer from the DNA ($k_{\text{off,DF}} = 0.026 \text{ s}^{-1}$). For the other datasets (AtARF2-FL K2S, AtARF2-FL OPCA, and AtARF2-DBD), the dissociation of the dimer from the DNA caused by the loss of a monomer plays a role and becomes almost as likely as the dissociation of the dimer from the DNA in the case of AtARF2-DBD ($k_{\text{off,DM}} = 0.016 \text{ s}^{-1}$).

The kinetic and equilibrium constants obtained from the global fit show that the monomer is the predominant species in solution for most of AtARF2 variants and for most of the tested concentration range (Fig. 2 D, Top, solid lines). Strikingly, the fraction of DNA bound by a monomer never exceeds 10% (Fig. 2 D, Top, dashed lines). The complex consisting of the AtARF2 dimer bound to the DNA can split by either a monomer or the dimer dissociating from the DNA. Our results show that the dissociation of the dimer from the DNA is the route used by AtARF2-FL and AtARF2-FL KpO, while the dissociation from the DNA through loss of a monomer becomes viable for AtARF2-FL K2S and OPCA and accounts for approximately 40% of the splitting events in the case of AtARF2-DBD (Fig. 2 D, Bottom).

Dimer Stability Determines the Binding Kinetics of ARF-DBDs.

We showed that AtARF2 dimer stability induced by the presence of the PB1 domain influences the kinetics of the binding of ARF toward its DNA response element. We next asked whether dimer stability is a more generic parameter defining DNA binding affinity across the ARF protein family. To this end, we purified the DNA-binding domains of two other ARFs (class B AtARF1-DBD and class A AtARF5-DBD) and two mutant versions (AtARF5-DBD

G279N and AtARF5-DBD R215A) and quantified their DNA binding affinity.

Experiments with AtARF1-DBD showed similar values of k_{on} and k_{off} ($1.3 \times 10^{-4} \text{ nM}^{-1} \text{ s}^{-1}$ 95% CI [0.8:1.8], 0.080 s^{-1} 95% CI [0.062:0.098], respectively) as AtARF2-DBD ($1.1 \times 10^{-4} \text{ nM}^{-1} \text{ s}^{-1}$ 95% CI [0.7:1.4], 0.066 s^{-1} 95% CI [0.045:0.087], respectively; Fig. 3). On the other hand, AtARF5-DBD showed a fivefold increase in k_{on} ($5.9 \times 10^{-4} \text{ nM}^{-1} \text{ s}^{-1}$ 95% CI [2.3:9.4]) and an eightfold reduction in k_{off} (0.0085 s^{-1} 95% CI [0.0051:0.0118]) compared to AtARF2-DBD; which led to a K_{d} of 15 nM (95% CI [12:18]). In analogy with the considerations made for AtARF2-FL, the increase in k_{on} and part of the decrease in k_{off} can be explained with AtARF5-DBDs forming a tighter dimer compared to AtARF1 and AtARF2 DBDs.

To test this hypothesis, we tested AtARF5-DBD G279N, a single amino acid mutation known to reduce AtARF5-DBD dimerization (19). Strikingly, the kinetics of the interaction between AtARF5-DBD G279N and the IR7 became similar to the ones of AtARF1 and AtARF2 DBDs ($1.2 \times 10^{-4} \text{ nM}^{-1} \text{ s}^{-1}$ 95% CI [1.0:1.5], 0.10 s^{-1} 95% CI [0.04:0.17]) validating our hypothesis. Finally, we tested AtARF5-DBD R215A, a mutant in which a key amino acid for the interaction with the DNA is mutated (19). This mutant showed a 13-fold reduction of k_{on} compared to the wild-type ($0.46 \times 10^{-4} \text{ nM}^{-1} \text{ s}^{-1}$ 95% CI [0.41:0.51]) as well as a 39-fold increase of k_{off} (0.33 s^{-1} 95% CI [0.14:0.52]) which translates in a reduction of affinity of three orders of magnitude. We note that the magnitude of the reduction of k_{on} is consistent with the effect of charge neutralization of DNA-contacting residues seen in other protein–DNA interactions (30) and is a reminder of the importance of charged residues in defining association kinetics (31, 32).

To directly measure ARF dimer stability, we measured SAXS (small-angle X-ray scattering) intensity profiles of AtARF5-DBD and AtARF1-DBD (Fig. 4). The difference in stability is clear with AtARF5-DBD exhibiting higher dimer prevalence at all tested concentrations. The results on AtARF5-DBD are consistent with a dimerization K_{d} in the order of the tenth of μM while for AtARF1-DBD the K_{d} is in the order of few μM. These results confirm the expectation set by the analysis of the binding kinetics that AtARF5-DBD forms relatively stable dimers even in absence of the PB1 domain.

Discussion

The ARF PB1 domain mediates the binding of Aux/IAA to ARF, allowing for the inhibition of ARF activity (3–5). In ARFs from Arabidopsis, deleting or mutating the PB1 domain leads to hyperactive ARFs (25), consistent with a role in suppressing activity. In contrast, the Marchantia ARF1 PB1 domain is required for a function; a deletion of this domain renders the protein inactive (24). Given that the minimal set of ARF proteins found in Marchantia qualifies these as likely representatives of ancestral

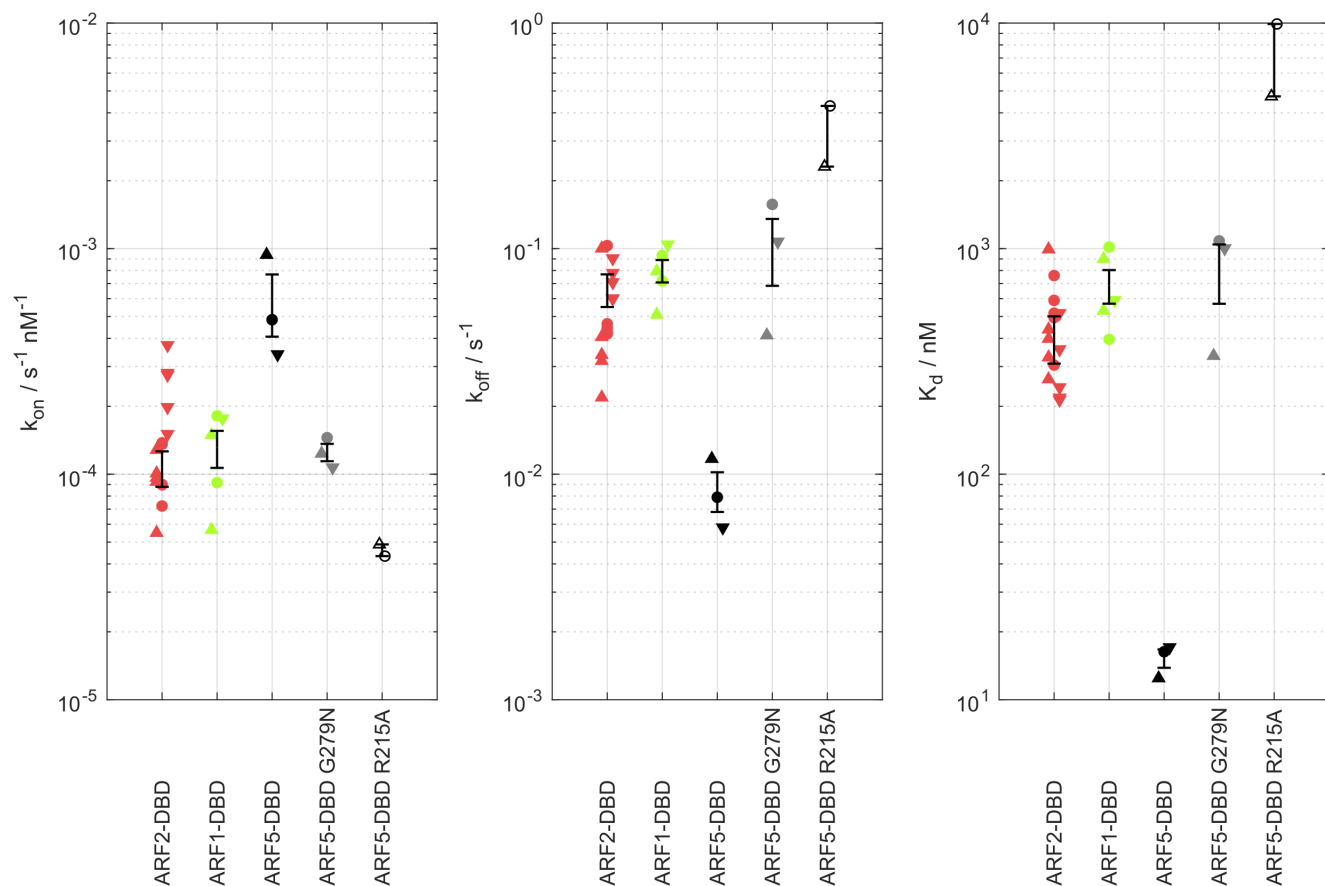


Fig. 3. Kinetics of the interaction between AtARF-DBDs and IR7. Kinetic parameters obtained from HMM analysis using ebFRET. The data points are marked with triangle, square and inverted triangle in order of increasing ARF concentration. The ARF concentrations were 128, 256, 512 nM for AtARF2-DBD and AtARF1-DBD, 8, 16 and 32 nM for AtARF5-DBD, 64, 128 and 256 nM for AtARF5-DBD G279N and 128 and 512 nM for AtARF5-DBD R215A. The error bars represent the SDs of the mean values. AtARF2-DBD and AtARF1-DBD behaved similarly while AtARF5-DBD showed increased k_{on} and decreased k_{off} . Consistent with a model in which part of the difference in kinetics can be explained by an increased stability of AtARF5-DBD dimer, weakening of AtARF5-DBD dimerization (G279N mutant) leads to kinetic parameters that resemble the ones of AtARF1-DBD and AtARF2-DBD. In addition, AtARF5-DBD R215A mutant in a key amino acid for the interaction with DNA showed a k_{on} reduced by one order of magnitude and a k_{off} increased by almost two orders of magnitude compared to the AtARF5-DBD wild-type.

protein functions (33), an open question is what the actual roles of ARF PB1 domains are. Here, we explored the role of this domain in modulating the DNA-binding affinity of AtARF2 toward an IR7 response element. We found that full-length AtARF2 protein has a strongly increased DNA-binding affinity, which can be ascribed to interactions between the PB1 domains. Interestingly, our results show that oligomerization does not

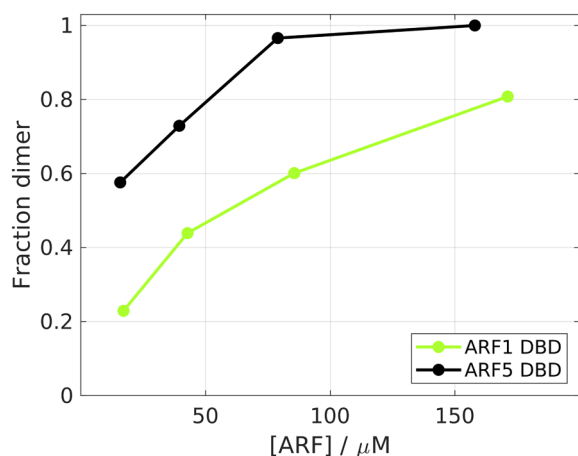


Fig. 4. Fraction of dimer measured using SAXS. The stability of the dimer of AtARF5-DBD is higher than the one of AtARF1-DBD for all tested concentration.

further enhance the affinity toward bipartite response elements, a result that mirrors findings in a heterologous yeast assay with AtARF19 (26). This behavior is consistent with the fact that additional ARF monomers (beside the initial two) do not have any AuxRE left to further stabilize the binding to the DNA. This said, the effect of the PB1 domain seen in our experiments predicts that oligomerization should be relevant on response elements comprising of more than two AuxREs as the PB1 domain would enable cooperative binding beyond the dimer. Given the short consensus sequence in AuxRE motifs, these may occur in close proximity in promoters, in which case oligomerization could generate additional cooperativity of ARF–DNA interaction. Regardless, the use of a C-terminal head-to-tail oligomerization domain (with two interaction faces) can be considered an efficient means of flexible interaction.

By simultaneously fitting affinity and kinetic data with the analytical solution of a four-state cyclic model, we showed that the increase of ARF DNA binding affinity can be completely attributed to a shift in the dimer/monomer equilibrium of ARFs. It follows that the effect of the PB1 domain on ARF affinity toward an IR7 response element is to shift the dimerization equilibrium toward the dimer. Strikingly, the fit allows obtaining quantitative information about the protein dimerization K_d in solution (i.e., K_f) although the protein was not directly observed in the experiment.

The kinetic parameters for AtARF2-DBD show that DNA binding and unbinding is almost equally probable to happen

through a monomer-bound DNA intermediate or through direct binding of the dimer (Fig. 5, *Left*). Moreover, the monomer is the most common species in solution even at ARF concentrations that saturate the DNA (i.e., DNA fully bound by an ARF dimer); despite this, the percentage of DNA bound by an ARF monomer never exceeds 10% as this intermediate is short-lived and quickly proceeds to either form a dimer or dissociate.

The kinetics of AtARF2-FL KpO-IR7 interaction is remarkably different (Fig. 5, *Right*); here, the association between the DNA and a dimer follows almost exclusively the pathway where the ARF dimer is formed in solution. Moreover, the unbinding of a single monomer from a dimer bound to the DNA is unlikely ($K_d < 1$ nM).

In general, the importance of dimerization for stable DNA binding clearly emerges from our analysis as a reminder of the importance of cooperativity in protein–DNA interactions. Moreover, cooperativity is symmetric: A protein that can dimerize on a bipartite response element will bind it with higher affinity but also a bipartite element will stabilize the dimer of the protein that is bound to it. In particular, the dimer of AtARF2 is ≈ 60 times more stable when bound to the DNA compared to being in solution.

The analysis of the kinetics of the interaction between different ARF DBDs and the IR7-RE suggests that the tighter binding of AtARF5-DBD compared to AtARF1 and AtARF2 DBDs is in part due to the higher stability of its dimer. This prediction is further corroborated by SAXS data showing that AtARF5-DBD forms more stable dimers in solution compared to AtARF1-DBD. The stable DNA binding that AtARF5-DBD achieves even in the absence of the PB1 domain could explain why AtARF5 Δ PB1 is a gain-of-function mutant that can activate auxin-responsive genes even in the absence of auxin (25). Then, the role of the PB1 domain of AtARF5 appears to be mainly to bind the PB1 domain of Aux/IAAs coupling the transcriptional output of ARF with the presence of auxin. This hypothesis is confirmed by the fact that the PB1 domain of AtARF5 has a homodimerization K_d of 870 nM but an heterodimerization K_d with the PB1 domain of Aux/IAA17 of 73 nM (8). Moreover, AtARF5 and other class A ARFs have been found to interact with many different Aux/IAA in a series of protein–protein interaction assays (26, 34–44). A different scenario is seen in case of AtARF2 (a class B ARF), where our data suggest that the interaction between PB1 of different AtARF2 monomers might be required to achieve the stable DNA binding that enables protein function. This behavior of the PB1 domain might be a common feature of other class B/C ARFs and could explain why this class of ARFs has been seen to interact with fewer

members of the Aux/IAA family (34, 42–45). It should be noted that additional domains beyond the DBD endow different ARFs with unique properties. For example, AtARF7 and AtARF19 were shown to form condensates through their MR (46). It will be interesting to see how well the findings here—based on isolated proteins—generalize across the ARF family. Furthermore, ARFs can be posttranslationally modified, e.g., through SUMOylation (47) or phosphorylation (48) and can bind other transcription factors (49, 50). It is an open question how such additional components modify the dimerization domain cooperativity in DNA binding. Lastly, a major limitation of the assays as presented is that they use short DNA elements and lack the natural nucleosome context. Incorporation of extended DNA templates, as for example in DNA curtains (51), perhaps even including histone proteins, would help translate in vitro dynamics to the cellular context.

The picture emerging is that the PB1 domain has different functions in the two main ARF classes in *A. thaliana*. In class A ARFs, it serves as a mediator of auxin-responsiveness, whereas it stabilizes the DNA binding in class B (and perhaps C) ARFs. This model of action for the PB1 domain is similar to the one found in *M. polymorpha* as part of the recently published minimal auxin response system (24) with one key difference: MpARF1 (the only class A ARF in this species) cannot function without its PB1 domain. Therefore, the PB1 domain of class A ARFs in *M. polymorpha* probably has the double function of stabilizing the binding to the DNA and interacting with MpAux/IAA. This double function opens the possibility of a double repression by Aux/IAA, where, in addition to the recruitment of the corepressor TOPLESS (52) (TPL), a destabilization of ARF–DNA interaction might also play a role.

Binding of ARF to bipartite AuxREs in the other two possible orientations (directed repeat DR and everted repeat ER) should resemble the one seen for the IR with the difference that the dimerization through the DBD domain should not be possible. In this scenario, the analytical solution of the four-state model for ARF-DBDs simplifies to a binding isotherm for independent binding of the monomers characterized by low steepness (no cooperativity, see also *SI Appendix, Note 1*). Strikingly, titrations presented in a recent publication (27) confirmed this prediction; the binding of AtARF1-DBD and AtARF5-DBD to a bipartite DR5 was compatible with a simple binding isotherm, whereas binding to an IR8 showed steeper response, similar to the one seen here for AtARF2-DBD. Since stable DNA binding arises from stable dimerization/oligomerization, the topology of composite AuxREs dictates the affinity toward distinct ARF members differentiating

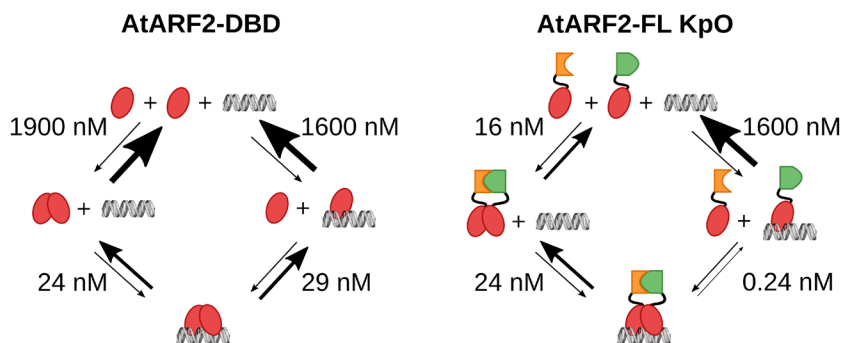


Fig. 5. Dissociation constants for the four-state cyclic model as determined from the fit in Fig. 2. AtARF2-DBD binds the DNA via dimerization on the DNA and dimerization in solution with similar probability. AtARF2-FL KpO mostly dimerizes in solution and then binds the DNA. The presence of the PB1 domain reduces all K_d s making all interactions more stable (aside from the monomer–DNA interaction). This results in the higher affinity of ARF toward the RE when the PB1 domain is present.

them based on the relative strength of the homotypic interaction through their DBD and PB1 domains. Tweaking the affinities of different ARFs toward the same DNA sequence can be achieved by affecting their dimerization properties and opens the possibility for an evolutionary pathway of complex interactions between members of the family.

Lastly, it is interesting to speculate on the biological significance of the dual, cooperative dimerization mode we identified here. Effectively, the double-check mechanism would favor dimerization of ARFs, when bound on DNA. ARF monomers have limited sequence specificity of DNA binding. In the hexanucleotide binding site, only 2 nucleotides are invariant, and four are conserved (18, 19, 53). Thus, one would expect a monomer to find binding sites frequently in the genome. Dimerization adds two constraints that dramatically increase specificity: a second, symmetric DNA element as well as a fixed optimal space between the elements. This strongly limits the probability of a random occurrence of the response element and explains why dimerization is such a common feature of transcription factors across all domains of life (54, 55). Unfortunately, probing genome-wide ARF binding has been challenging, and no comparisons between monomers and dimers have yet been made. However, ARF2 and ARF5 have both been used in DAP-seq binding site mapping on the Arabidopsis genome (18). If dimerization limits the number of genomic binding sites, one would predict that ARF5 with a higher propensity to dimerize (as shown here) binds fewer sites. This is exactly what was found: ARF2 appears more promiscuous in its binding profile (18, 53). A hypothesis, to be tested in the future, is therefore that dimerization is the primary mechanism for defining ARF–DNA binding specificity in vivo.

Materials and Methods

Protein Expression and Purification. Protein expression and purification were carried out as described previously (19). Briefly, the genomic regions corresponding to the DNA binding domain (DBD) of *A. thaliana* ARF1, ARF2, ARF5, and full-length ARF2 were amplified and cloned in a modified expression vector pTWIN1 (New England Biolabs) to generate fusions with the Chitin Binding Domain (CBD) and Intein. ARF–CBD fusion proteins were expressed in *Escherichia coli* strain Rosetta DE3 (Novagen). Cells were inoculated in Difco Terrific Broth (BD), supplemented with ampicillin, and grown to an OD_{600} of 0.5 to 0.7, protein expression was induced by adding isopropyl β -D-thiogalactopyranoside (IPTG), and the temperature was switched from 37 °C to 20 °C; the growth was continued for 20 h. Cells were harvested by centrifugation and resuspended in a 50-mL extraction buffer (20 mM Tris, 500 mM NaCl, 1 mM EDTA, 0.1% NP-40 and 2 mM $MgCl_2$, pH 7.8, 10 mg of DNase, and 0.2 mM phenylmethylsulfonyl fluoride [PMSF]). Cells were then lysed by passing the suspension twice through a French Pressure cell press, and cell-free extract was generated by centrifugation. The supernatant was loaded onto a chitin column (New England Biolabs) and washed with 10-column volumes washing buffer (20 mM Tris, 500 mM NaCl, pH 7.8) using an AKTA explorer 100 (GE Healthcare). ARF–DBD proteins were eluted by 1 h incubation with 40 mM dithiothreitol (DTT) in washing buffer. Proteins were concentrated using Amicon ultra-15 10K spin filters and next passed over a Superdex 200PG size-exclusion chromatography column. ARF–DBD proteins were eluted using washing buffer with 1 mM DTT, concentrated using Amicon ultra-15 10K spin filters, and stored until use at -80 °C.

DNA Constructs. Single-strand DNA oligonucleotides were ordered from Eurogentec. Each strand contained a 5-C6-amino-dT modification at the desired position for labeling. Some of the strands were purchased biotinylated at their 5'-end to allow for surface immobilization using a Neutravidin bridge. Strands were labeled with the desired dye (Cy3 or ATTO 647N NHS-ester) following a modified version of the protocol provided by the dye manufacturer and purified using polyacrylamide gel electrophoresis (20% Acrylamide). DNA constructs were annealed by heating complementary single strands to 95 °C in annealing buffer

(250 mM NaCl, 10 mM Tris HCl pH 8, 1 mM EDTA) followed by cooling down to room temperature overnight.

Single-Molecule FRET. Imaging was carried out on a home-built TIRF microscope, described previously (56). The measurements were performed using alternating-laser excitation (ALEX) (57); in this excitation scheme, each frame during which the donor is excited is followed by a frame in which the acceptor is directly excited. The emission of the fluorophores is spectrally divided into two different detection channels on the emCCD camera sensor (Andor iXon 897 Ultra). This approach creates four photon streams, three of which are relevant: (1) donor emission after donor excitation (DD), (2) acceptor emission after donor excitation (DA, arising from FRET), and (3) acceptor emission after acceptor excitation (AA). The three photon streams can be used to calculate the raw FRET efficiency ($E^* = DA / (DD + DA)$) and stoichiometry ($S^* = (DD + DA) / (DD + DA + AA)$) (58). E^* contains the information about the relative distance of the two fluorophores, whereas S^* contains information about the photophysical state of a given molecule (allowing to filter out molecules missing an active donor or an active acceptor).

We note that the donor fluorophore used in our experiment (Cy3) exhibits an increase in quantum yield when in close proximity to a protein, an effect known as protein-induced fluorescent enhancement (PIFE) (57, 59–62). This effect can be observed in smFRET experiments using ALEX excitation scheme; since the donor becomes brighter compared to the acceptor, the stoichiometry increases (SI Appendix, Fig. S2). This change in stoichiometry can be used to infer the binding state of the DNA construct but its value proved too small to provide reliable information. For this reason, we limited our analysis to the change in FRET efficiency.

The camera acquisition time and the excitation time were set to 250 ms per frame; laser powers were set to 3 mW for green ($\lambda = 561$ nm) and 0.5 mW for red ($\lambda = 638$ nm) lasers. The phosphate-buffered saline (PBS) imaging buffer (pH 7.4) contained 137 mM NaCl, 2.7 mM KCl, 10 mM phosphate, and 1 mM Trolox, 1% glyco, and 1% glucose to decrease the rate of photobleaching (63, 64).

Single-Molecule Titration Experiments. Labeled dsDNA oligos were immobilized on a PEGylated glass coverslip as described previously (65). In particular, the PEGylation was carried out inside the wells of silicone gaskets placed on the coverslip (Grace Bio-labs). Each protein titration was performed using a single well, washing it between data points with 600 μ L of $1 \times$ PBS buffer. The final washing step consisted of three washings separated by 15 min. Typically, each data point consisted of four movies (1,000 frames each).

Binding Isotherms Analysis. The fit of the FRET efficiency distribution with the two Gaussian distributions pertaining to the free and ARF-bound DNA populations returns an uncorrected fraction of ARF-bound DNA for each tested protein concentration i : $F_B^u(i)$. Even when no protein is added, the double Gaussian fit returns an uncorrected fraction-bound $F_B^u(0) > 0$ (typically ≈ 0.1). This value is an indication of the error connected to the two-population fit and can be used to renormalize the entire titration under the assumption that, in case the DNA would be completely bound by ARF, the expected uncorrected free fraction would have the same value ($F_B^u(0) = F_B^u(\infty)$). Then, the corrected fraction bound for each protein concentration can be calculated as:

$$F_B^c(i) = \frac{F_B^u(i) - F_B^u(0)}{1 - 2F_B^u(0)}.$$

The corrected fraction bound (henceforth F_B) can be fit with the appropriate mathematical model for the interaction.

Time Traces Analysis. First, the time traces from individual DNA molecules were filtered to remove sections in which either the donor or the acceptor fluorophore were inactive due to fluorophore bleaching or blinking. Each molecule was allowed to take values of E^* and S^* outside the thresholds (typically 0 to 0.85 for E^* and 0.5 to 0.9 for S^*) for a maximum of three consecutive data points; longer stays outside the thresholding range resulted in the trace being interrupted. In case the molecule reentered the allowed range for E^* and S^* , the data points were saved as a new trace. The minimum length of traces was set to 50 data points (100 frames). The filtered time traces were then loaded in the software package ebFRET to perform an empirical Bayes Hidden Markov Modelling (29). The analysis was

performed assuming two states, with two restarts and a convergence threshold of 1×10^{-6} . The results of the analysis were exported as '.csv' text files, and the transition matrix was used to calculate k_{on} and k_{off} . The K_d was calculated as $k_{\text{off}}/k_{\text{on}}$.

SAXS Analysis. Different concentrations of AtARF1 and AtARF5 ranging from 17 μM to 170 μM (0.7 mg/mL to 7 mg/mL) were tested to record ARF dimerization depending on protein concentration. All the samples were prepared in a final buffer consisting of 20 mM Tris-HCl pH 8.0, 150 mM NaCl, 1 mM DTT. SAXS data were collected at NCD-SWEET beamline (BL11, ALBA Synchrotron, Barcelona) (66, 67). The buffer was collected for subtraction of protein samples. Measurements were carried out at 293 K in a quartz capillary of 1.5 mm outer diameter and 0.01 mm wall thickness. The data (20 frames with an exposure time of 0.5 s/frame) was recorded using a Pilatus 1M detector (Dectris, Switzerland) at a sample-detector distance of 2.56 m and a wavelength of 1.0 Å.

Buffer subtraction and extrapolation to infinite dilution were performed by using the program package primus/qt from the ATSAS 2.8.4 software suite (68). The forward scattering $I(Q)$ and the radius of gyration (R_g) were evaluated by

1. P. Grones, J. Friml, Auxin transporters and binding proteins at a glance. *J. Cell Sci.* **128**, 1–7 (2015).
2. M. Lavy, M. Estelle, Mechanisms of auxin signaling. *Development* **143**, 3226–3229 (2016).
3. D. Weijers, D. Wagner, Transcriptional responses to the auxin hormone. *Annu. Rev. Plant Biol.* **67**, 539–574 (2016).
4. F. Parcy, T. Vernoux, R. Dumas, A glimpse beyond structures in auxin-dependent transcription. *Trends Plant Sci.* **21**, 574–583 (2016).
5. M. Roosjen, S. Pague, D. Weijers, Auxin response factors: Output control in auxin biology. *J. Exp. Bot.* **69**, 179–188 (2018).
6. M. H. Nanao *et al.*, Structural basis for oligomerization of auxin transcriptional regulators. *Nat. Commun.* **5**, 3617 (2014).
7. D. A. Korasick *et al.*, Molecular basis for AUXIN RESPONSE FACTOR protein interaction and the control of auxin response repression. *Proc. Natl. Acad. Sci. U.S.A.* **111**, 5427–5432 (2014).
8. M. Han *et al.*, Structural basis for the auxin-induced transcriptional regulation by Aux/IAA17. *Proc. Natl. Acad. Sci. U.S.A.* **111**, 18613–18618 (2014).
9. D. C. Dinesh *et al.*, Solution structure of the PslAA4 oligomerization domain reveals interaction modes for transcription factors in early auxin response. *Proc. Natl. Acad. Sci. U.S.A.* **112**, 6230–6235 (2015).
10. T. Ulmasov, G. Hagen, T. J. Guilfoyle, Activation and repression of transcription by auxin-response factors. *Proc. Natl. Acad. Sci. U.S.A.* **96**, 5844–5849 (1999).
11. S. B. Tiwari, G. Hagen, T. Guilfoyle, The roles of auxin response factor domains in auxin-responsive transcription. *Plant Cell* **15**, 533–543 (2003).
12. T. Ulmasov, G. Hagen, T. J. Guilfoyle, ARF1, a transcription factor that binds to auxin response elements. *Science* **276**, 1865–1868 (1997).
13. N. Ballas, L.-M. Wong, A. Theologis, Identification of the auxin-responsive element, AuxRE, in the primary indoleacetic acid-inducible gene, PS-IAA4/5, of pea (*Pisum sativum*). *J. Mol. Biol.* **233**, 580–596 (1993).
14. Y. Li, Z.-B. Liu, X. Shi, G. Hagen, T. J. Guilfoyle, An auxin-inducible element in soybean SAUR promoters. *Plant Physiol.* **106**, 37–43 (1994).
15. T. Ulmasov, Z. B. Liu, G. Hagen, T. J. Guilfoyle, Composite structure of auxin response elements. *Plant Cell* **7**, 1611–1623 (1995).
16. T. Ulmasov, G. Hagen, T. J. Guilfoyle, Dimerization and DNA binding of auxin response factors. *Plant J.* **19**, 309–319 (1999).
17. J. M. Franco-Zorrilla *et al.*, DNA-binding specificities of plant transcription factors and their potential to define target genes. *Proc. Natl. Acad. Sci. U.S.A.* **111**, 2367–2372 (2014).
18. R. C. O'Malley *et al.*, Cistrome and epistemic features shape the regulatory DNA landscape. *Cell* **165**, 1280–1292 (2016).
19. D. R. Boer *et al.*, Structural basis for DNA binding specificity by the auxin-dependent ARF transcription factors. *Cell* **156**, 577–589 (2014).
20. C.-Y. Liao *et al.*, Reporters for sensitive and quantitative measurement of auxin response. *Nat. Methods* **12**, 207–210 (2015).
21. J. Liu *et al.*, Natural variation in ARF18 gene simultaneously affects seed weight and silique length in polyploid rapeseed. *Proc. Natl. Acad. Sci. U.S.A.* **112**, E5123–E5132 (2015).
22. A. Lancot, M. Taylor-Teeple, E. A. Oki, J. L. Nemhauser, Specificity in auxin responses is not explained by the promoter preferences of activator ARFs1. *Plant Physiol.* **182**, 1533–1536 (2020).
23. M. Galli *et al.*, The DNA Binding landscape of the maize AUXIN RESPONSE FACTOR family. *Nat. Commun.* **9**, 4526 (2018).
24. H. Kato *et al.*, Design principles of a minimal auxin response system. *Nat. Plants* **6**, 473–482 (2020).
25. N. T. Krogan, W. Kukurshumova, D. Marcos, A. E. Caragea, T. Berleth, Deletion of MP/ARF5 domains III and IV reveals a requirement for Aux/IAA regulation in Arabidopsis leaf vascular patterning. *New Phytol.* **194**, 391–401 (2012).
26. E. Pierre-Jerome, B. L. Moss, A. Lancot, A. Hageman, J. L. Nemhauser, Functional analysis of molecular interactions in synthetic auxin response circuits. *Proc. Natl. Acad. Sci. U.S.A.* **113**, 11354–11359 (2016).
27. A. Freire-Rios *et al.*, Architecture of DNA elements mediating ARF transcription factor binding and auxin-responsive gene expression in Arabidopsis. *Proc. Natl. Acad. Sci. U.S.A.* **117**, 24557–24566 (2020).
28. D. Colquhoun, K. A. Dowsland, M. Beato, A. J. R. Plested, How to impose microscopic reversibility in complex reaction mechanisms. *Biophys. J.* **86**, 3510–3518 (2004).
29. J.-W. van de Meent, J. E. Bronson, C. H. Wiggins, R. L. Gonzalez, Empirical bayes methods enable advanced population-level analyses of single-molecule FRET experiments. *Biophys. J.* **106**, 1327–1337 (2014).
30. S. P. Hancock, D. A. Hiller, J. J. Perona, L. Jen-Jacobson, The energetic contribution of induced electrostatic asymmetry to DNA bending by a site-specific protein. *J. Mol. Biol.* **406**, 285–312 (2011).
31. G. Schreiber, G. Haran, H.-X. Zhou, Fundamental aspects of protein–protein association kinetics. *Chem. Rev.* **109**, 839–860 (2009).
32. H.-X. Zhou, X. Pang, Electrostatic interactions in protein structure, folding, binding, and condensation. *Chem. Rev.* **118**, 1691–1741 (2018).
33. S. K. Mutte *et al.*, Origin and evolution of the nuclear auxin response system. *eLife* **7**, e33399 (2018).
34. F. Ouellet, P. J. Overvoorde, A. Theologis, IAA17/AXR3: Biochemical insight into an auxin mutant phenotype. *Plant Cell* **13**, 829–841 (2001).
35. T. Hamann, E. Benkova, I. Bäurle, M. Kientz, G. Jürgens, The Arabidopsis BODENLOS gene encodes an auxin response protein inhibiting MONOPTEROS-mediated embryo patterning. *Genes. Dev.* **16**, 1610–1615 (2002).
36. K. Tatematsu *et al.*, MASSUGU2 encodes Aux/IAA19, an Auxin-regulated protein that functions together with the transcriptional activator NPH4/ARF7 to regulate differential growth responses of hypocotyl and formation of lateral roots in Arabidopsis thaliana. *Plant Cell* **16**, 379–393 (2004).
37. C. S. Hardtke *et al.*, Overlapping and non-redundant functions of the Arabidopsis auxin response factors MONOPTEROS and NONPHOTOTROPIC HYPOCOTYL4. *Development* **131**, 1089–1100 (2004).
38. D. Weijers *et al.*, Developmental specificity of auxin response by pairs of ARF and Aux/IAA transcriptional regulators. *EMBO J.* **24**, 1874–1885 (2005).
39. H. Fukaki, Y. Nakao, Y. Okushima, A. Theologis, M. Tasaka, Tissue-specific expression of stabilized SOLITARY-ROOT/IAA14 alters lateral root development in Arabidopsis. *Plant J.* **44**, 382–395 (2005).
40. H. Muto *et al.*, Fluorescence cross-correlation analyses of the molecular interaction between an Aux/IAA protein, MSG2/IAA19, and protein-protein interaction domains of auxin response factors of Arabidopsis expressed in HeLa cells. *Plant Cell Physiol.* **47**, 1095–1101 (2006).
41. T. Uehara, Y. Okushima, T. Mimura, M. Tasaka, H. Fukaki, Domain II mutations in CRANE/IAA18 suppress lateral root formation and affect shoot development in Arabidopsis thaliana. *Plant Cell Physiol.* **49**, 1025–1038 (2008).
42. C. Shen *et al.*, Functional analysis of the structural domain of ARF proteins in rice (*Oryza sativa* L.). *J. Exp. Bot.* **61**, 3971–3981 (2010).
43. T. Vernoux *et al.*, The auxin signalling network translates dynamic input into robust patterning at the shoot apex. *Mol. Systems Biol.* **7**, 508 (2011).
44. S. Piya, S. K. Shrestha, B. Binder, C. N. J. Stewart, T. Hwezi, Protein-protein interaction and gene co-expression maps of ARFs and Aux/IAAs in Arabidopsis. *Front. Plant Sci.* **5** (2014).
45. T. Ulmasov, J. Muffett, G. Hagen, T. J. Guilfoyle, Aux/IAA proteins repress expression of reporter genes containing natural and highly active synthetic auxin response elements. *Plant Cell* **9**, 1963–1971 (1997).
46. S. K. Powers *et al.*, Nucleo-cytoplasmic partitioning of ARF proteins controls auxin responses in Arabidopsis thaliana. *Mol. Cell* **76**, 177–190.e5 (2019).
47. B. Orosa-Puente *et al.*, Root branching toward water involves posttranslational modification of transcription factor ARF7. *Science* **362**, 1407–1410 (2018).
48. H. Cho *et al.*, A secreted peptide acts on BIN2-mediated phosphorylation of ARFs to potentiate auxin response during lateral root development. *Nat. Cell Biol.* **16**, 66–76 (2014).
49. R. Shin *et al.*, The Arabidopsis transcription factor MYB77 modulates auxin signal transduction. *Plant Cell* **19**, 2440–2453 (2007).
50. E. Varaud *et al.*, AUXIN RESPONSE FACTOR8 regulates Arabidopsis petal growth by interacting with the bHLH transcription factor BIGPETALp. *Plant Cell* **23**, 973–983 (2011).
51. M.-L. Visnapuu, E. C. Greene, Single-molecule imaging of DNA curtains reveals intrinsic energy landscapes for nucleosome deposition. *Nat. Struct. Mol. Biol.* **16**, 1056–1062 (2009).
52. H. Szemenyei, M. Hannon, J. A. Long, TOPLESS mediates auxin-dependent transcriptional repression during Arabidopsis embryogenesis. *Science* **319**, 1384–1386 (2008).
53. A. Stigliani *et al.*, Capturing auxin response factors in situ using DNA binding models. *Molecular Plant* **12**, 822–832 (2019).
54. G. D. Amoutzias, D. L. Robertson, Y. Van de Peer, S. G. Oliver, Choose your partners: Dimerization in eukaryotic transcription factors. *Trends Biochem. Sci.* **33**, 220–229 (2008).
55. L. Strader, D. Weijers, D. Wagner, Plant transcription factors—Being in the right place with the right company. *Curr. Opin. Plant Biol.* **65**, 102136 (2022).
56. S. Farooq, J. Hohlbein, Camera-based single-molecule FRET detection with improved time resolution. *Phys. Chem. Chem. Phys.* **17**, 27862–27872 (2015).
57. J. Hohlbein, T. D. Craggs, T. Cordes, Alternating-laser excitation: Single-molecule FRET and beyond. *Chem. Soc. Rev.* **43**, 1156–1171 (2014).
58. A. N. Kapanidis *et al.*, Fluorescence-aided molecule sorting: Analysis of structure and interactions by alternating-laser excitation of single molecules. *Proc. Natl. Acad. Sci. U.S.A.* **101**, 8936–8941 (2004).
59. H. Hwang, H. Kim, S. Myong, Protein induced fluorescence enhancement as a single molecule assay with short distance sensitivity. *Proc. Natl. Acad. Sci. U.S.A.* **108**, 7414–7418 (2011).

the Guinier approximation, and the maximum distance D_{max} of the particle was also computed from the entire scattering patterns with AutoGNOM. The excluded volume V_p of the particle was computed from the Porod invariant. The scattering from the crystallographic models was computed with CRY SOL (69). The volume fractions of the oligomers were determined with OLIGOMER (70), using as probe the available PDB structures.

Data, Materials, and Software Availability. Raw measurement data have been deposited in Zenodo (<https://doi.org/10.5281/zenodo.7249508>).

ACKNOWLEDGMENTS. We would like to thank all our colleagues at the Laboratory of Biophysics and the Laboratory of Biochemistry for helpful discussions.

Author affiliations: ^aLaboratory of Biophysics, Wageningen University and Research, 6708 WE Wageningen, The Netherlands; ^bLaboratory of Biochemistry, Wageningen University and Research, 6708 WE Wageningen, The Netherlands; ^cALBA synchrotron Light Source, Cerdanyola del Vallès, Barcelona 08290, Spain; and ^dMicrospectroscopy Research Facility, Wageningen University and Research, 6708 WE Wageningen, The Netherlands

60. E. M. S. Stennett, M. A. Ciuba, S. Lin, M. Levitus, Demystifying PIFE: The photophysics behind the protein-induced fluorescence enhancement phenomenon in Cy3. *J. Phys. Chem. Lett.* **6**, 1819–1823 (2015).
61. E. Ploetz *et al.*, Förster resonance energy transfer and protein-induced fluorescence enhancement as synergetic multi-scale molecular rulers. *Sci. Rep.* **6**, 33257 (2016).
62. E. Lerner, E. Ploetz, J. Hohlbein, T. Cordes, S. Weiss, A quantitative theoretical framework for PIFE-FRET. *J. Phys. Chem. B* **120**, 6401–6410 (2016).
63. I. Rasnik, S. A. McKinney, T. Ha, Nonblinking and long-lasting single-molecule fluorescence imaging. *Nat. Methods* **3**, 891–893 (2006).
64. T. Cordes, J. Vogelsang, P. Tinnefeld, On the mechanism of trolox as antiblinking and antibleaching reagent. *J. Am. Chem. Soc.* **131**, 5018–5019 (2009).
65. G. W. Evans, J. Hohlbein, T. Craggs, L. Aigrain, A. N. Kapanidis, Real-time single-molecule studies of the motions of DNA polymerase fingers illuminate DNA synthesis mechanisms. *Nucleic Acids Res.* **43**, 5998–6008 (2015).
66. J. González Fernández, "NCD-SWEET beamline upgrade" in *Proceedings of the Mechanical Eng. ~ Design of Synchrotron Radiation Equipment and Instrumentation MEDSI2018*, (2018), p. 3, 1.986 MB.
67. N. Gonzalez, "Beam conditioning optics at the ALBA NCD-SWEET beamline" in *Proceedings of the Mechanical Eng. ~ Design of Synchrotron Radiation Equipment and Instrumentation MEDSI2018*, (2018), p. 3, 0.688 MB.
68. D. Franke *et al.*, ATLAS 2.8: A comprehensive data analysis suite for small-angle scattering from macromolecular solutions. *J. Appl. Crystallogr.* **50**, 1212–1225 (2017).
69. D. Svergun, C. Barberato, M. H. J. Koch, CRYSOLE-A program to evaluate X-ray solution scattering of biological macromolecules from atomic coordinates. *J. Appl. Cryst.* **28**, 768–773 (1995).
70. P. V. Konarev, V. V. Volkov, A. V. Sokolova, M. H. J. Koch, D. I. Svergun, PRIMUS: A Windows PC-based system for small-angle scattering data analysis. *J. Appl. Cryst.* **36**, 1277–1282 (2003).